

Brillouin scattering in hybrid optophononic Bragg micropillar resonators at 300 GHz: supplementary material

M. ESMANN,¹ F. R. LAMBERTI,¹ A. HAROURI,¹ L. LANCO,¹ I. SAGNES,¹ I. FAVERO,² G. AUBIN,¹ C. GOMEZ-CARBONELL,¹ A. LEMAITRE,¹ O. KREBS,¹ P. SENELLART,¹ N. D. LANZILLOTTI-KIMURA^{1,*}

¹Centre de Nanosciences et de Nanotechnologies, Centre National de la Recherche Scientifique, Université Paris-Sud, Université Paris-Saclay, 10 Boulevard Thomas Gobert, 91120 Palaiseau, France

²Matériaux et Phénomènes Quantiques, CNRS UMR 7162, Université Paris Diderot, 75013 Paris, France

*Corresponding author: daniel.kimura@c2n.upsaclay.fr

Published 5 July 2019

This document provides supplementary information to “Brillouin scattering in hybrid optophononic Bragg micropillar resonators at 300 GHz,” <https://doi.org/10.1364/OPTICA.6.000854>. In this document, we present the photoelastic model used to simulate the anti-Stokes Brillouin scattering cross-section in planar and micropillars structures, additional measurements on the polarization dependence of the Brillouin signal in micropillars and further details on the spatial filtering technique developed to probe the confined acoustic phonons in the optophononic resonators.

51. Photoelastic model of the anti-Stokes Brillouin scattering cross-section

To model the Brillouin anti-Stokes scattering cross-section $I(\omega_l + \omega_p)$, we base our simulations on a transfer matrix implementation of a one-dimensional photoelastic model. For the photoelastic interaction, we consider the following overlap integral¹:

$$I(\omega_l + \omega_p) \propto \left| \int_{-\infty}^{\infty} E_{laser}(z, \omega_l) E_{scat}^*(z, \omega_l + \omega_p) \frac{\partial u(z, \omega_p)}{\partial z} p(z, \omega_l) dz \right|^2 \quad (1)$$

where ω_l is the frequency of the excitation laser. Here, $\frac{\partial u(z, \omega_p)}{\partial z}$ denotes the normal strain in the z-direction induced by the mechanical mode at a frequency ω_p . $E_{laser}(z, \omega_l)$ and $E_{scat}(z, \omega_l + \omega_p)$ are the incident and the Brillouin-scattered optical fields, and $p(z, \omega_l)$ is the p_{12} component of the photoelastic tensor. Note that at room temperature the fundamental electronic transition in GaAs is at 1.52 eV, such that the experiments are performed under nearly-resonant conditions. The Brillouin spectrum is thus dominated by the photoelastic contributions from the GaAs layers.

This 1D model has been successfully used in the case of planar structures¹⁻⁷. In the case of micropillars, we apply the following simplifications:

- 1) The longitudinal acoustic field is confined in the vertical direction so only one component of the acoustic field is considered.
- 2) The only relevant components of the photoelastic tensor are p_{11} and p_{12} ⁸. To simplify the model we assume a single generic value p_{12} taking into account that the acoustic phonons considered here are purely longitudinal.
- 3) The electric field profile has a vertical distribution identical to the planar case, and the radial modulation only introduces an envelope.

Moreover, we consider that the spatial profiles for the incoming photons $E_{laser}(z, \omega_l)$ (excitation) and the emitted photons $E_{scat}^*(z, \omega_l + \omega_p)$ (Brillouin) are identical, since the frequency shift induced by the longitudinal phonons is small when compared to the considered optical frequencies, so the expression for the electric fields simplifies to $|E_{laser}(z, \omega_l)|^2$.

For the materials GaAs and AlAs we use the following well-established optical and elastic parameters at room temperature:

	Speed of sound (m/s)	Density (kg/m ³)	Refractive index
GaAs	4780	5350	3.5373
AlAs	5660	3770	2.9624

Table S1: Acoustic and optical parameters used in the design of micropillar cavity devices discussed in the manuscript.

Using the integral in Eq. (1) in conjunction with the values tabulated above, we reach good agreement between calculation and experimental results for both planar structures and micropillars, as shown in Figure 2 of the main text.

The major design consideration for the Brillouin frequencies explored in this work are the layer thicknesses of the two acoustic distributed Bragg reflectors (DBRs) formed by 16 periods of 7.3nm/9.8nm (8.5nm/8.2nm) GaAs/AlAs layers. With the parameters tabulated in S1 these thicknesses are chosen such that each layer pair corresponds to half a wavelength of acoustic path at a phonon frequency of 320GHz. That is, an acoustic bandgap appears centered at this frequency. The particular combination of two DBRs supports the formation of a confined state at their interface³⁹. This is the confined phonon mode leading to the formation of the main Brillouin peak in the experimental spectra reported in our work.

The validity of our modelling is reflected in its correct prediction of both the position, frequency difference and even relative height of the different contribution to the Brillouin spectra measured on micropillar devices.

S2. Polarization dependence of the Brillouin signal

We have measured the polarization of the Brillouin emission. To this end, we ensured linear polarization of the incident laser and recorded spontaneous Brillouin spectra after transmission through a second analyzing polarizer, which was placed between the spatial filtering aperture and the entrance to the spectrometer (see schematic in Figure 1 of the main text). In Figure S1 below we show the measured Brillouin intensity (more precisely the integrated area of the main Brillouin peak) as a function of the analyzer angle and superimposed the result with a \cos^2 fit. We observe that the Brillouin emission is linearly polarized along the laser with a degree of polarization larger than 99%.

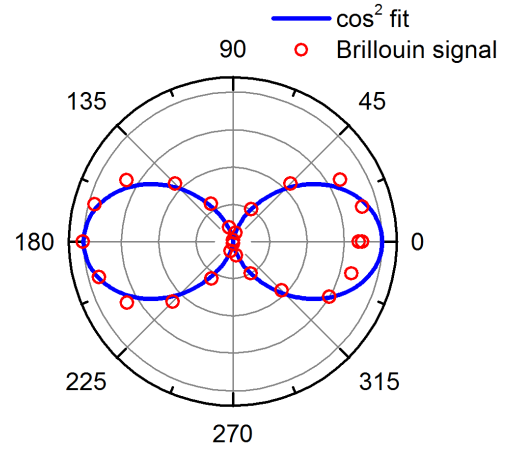


Figure S1: Polarization of Brillouin emission upon linear optical excitation. Displayed is the area under the central peak of the Brillouin spectrum. The degree of linear polarization in the Brillouin emission is larger than 99%.

S3. Spatial filtering of the Brillouin signals in planar and pillar microcavities

Since the Brillouin signal is resonantly coupled out of our device through to the fundamental micropillar mode, the spatial emission pattern of the Brillouin beam corresponds to the emission profile of the micropillar mode. The optical modes of micropillar cavities have been extensively studied in the context of single photon emitters and polaritonic systems and it has been shown that the characteristic emission is almost identical to the mode of an optical fiber, i.e. a Gaussian beam¹⁰⁻¹⁴.

In fact, the existence of a well-defined Brillouin beam is an important consideration in order to understand the working principle of the novel filtering technique. The latter is based on the use of a spatial filter, which is located close to the back-focal plane. Only due to the difference between the Gaussian spatial pattern of the micropillar mode and the ring-type pattern resulting from the diffracted excitation laser, we are able to spatially separate the two and isolate part of the spontaneous Brillouin scattering signal.

To further illustrate this point, the two sketches in Fig. S2 compare the experimental configuration on a micropillar and a planar microcavity, which was used for comparison in our study. Figure S2 (b) shows the configuration on a micropillar with the Gaussian Brillouin beam emerging from the resonator superimposed with the ring-shaped laser diffraction pattern. Figure S2 (a) shows the corresponding geometry on a planar structure. Here, the laser impinging under normal incidence with a small opening angle is not diffracted, but reflected back on its original path. The part of the laser which enters the cavity and interacts with the high frequency acoustic superlattice structure leads to the generation of a Brillouin signal at 320GHz. Instead of a discrete set of optical modes, the resonance energy of a planar optical microcavity shows a continuous parabolic dependence on the incidence angle. If the laser is thus resonant with the cavity under normal incidence, the Brillouin signal frequency-shifted by 320GHz from the laser will exhibit a resonance at a finite angle of incidence. This phenomenon is usually termed a double optical resonance (DOR) and has been employed to enhance Raman and Brillouin signals in planar configurations.^{6,7,15}

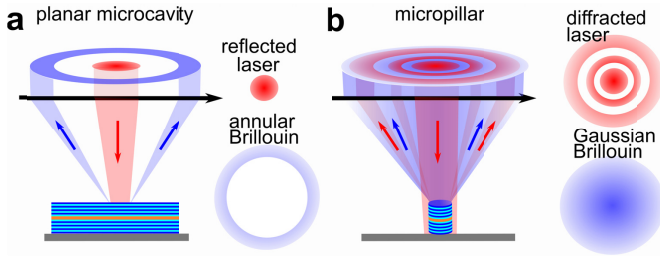


Figure S2 : **(a)** Brillouin scattering in a double optical resonance (DOR) configuration on a planar microcavity. While the incident laser (red) resonantly couples into the cavity under normal incidence, the frequency-shifted Brillouin signal (blue) is resonantly emitted under an angle. This allows, in principle, perfect spatial filtering in a plane behind the collection lens. **(b)** Brillouin scattering on a micropillar resonator. The incident laser resonantly couples to the optical micropillar mode. Its cross-section is chosen such that it leads to the formation of a dominant diffraction pattern in back reflection. In contrast, the Brillouin signal solely emerges through the fundamental micropillar mode with a Gaussian mode pattern. This allows near-perfect filtering in a plane behind the collection lens with a spatial filter exclusively transmitting in a diffraction node.

In the studied case, we employ the same spatial filter used on the micropillar to isolate the Brillouin signal on the planar reference structure. Since the numerical aperture of the incident laser beam is small, the directly reflected contribution can be completely blocked by the spatial filter. The resonant Brillouin signal emerging in a cone is collected and analyzed in a spectrometer.

S4. Brillouin backscattering in superlattices

To determine Brillouin backscattering frequencies in the semiconductor superlattices S1 and S2 of our sample, one needs to account for the folding of the acoustic superlattice band structure back into its first Brillouin zone. This folding induces multiple solutions of the Brillouin backscattering condition $k_p = 2k_l$ with k_p the quasi-momentum of the corresponding Bloch modes. This general aspect of Brillouin scattering in acoustic superlattices is illustrated in Figure S3 below.

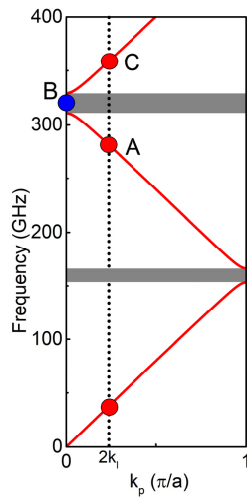


Figure S3: Acoustic phonon band structure of a nanophononic superlattice. Displayed are the three lowest bands separated by acoustic minigaps around 160GHz and 320GHz. The dashed vertical line marks the laser momentum $2k_l$. Intersections with the acoustic bands for which the Brillouin backscattering condition $k_p = 2k_l$ is fulfilled are found around 30GHz, 280GHz and 360GHz. The same labels A-C as in Figure 2 of the main text are used to mark the three acoustic phonon modes observed in our experiments.

The band structure exhibits isolated bands of propagating phonon modes separated by acoustic minigaps. The minigap centers occur at integer multiples of $f_0 = 160\text{GHz}$, at the zone edges and at the zone centers of the reduced Brillouin zone. For these frequencies the acoustic thickness of the lattice unit cell is an integer multiple of $\lambda_p/2$ with λ_p the phonon wavelength. The edges of the Brillouin zone at quasi-momentum $k_{edge} = \pm\pi/a$ are determined by a , the geometric thickness a of the superlattice unit cell. The dashed vertical line marks $2k_l$ and intersects once with each acoustic band. Each band of an acoustic superlattice hence contributes one peak to the Brillouin spectrum. The parameters chosen in the calculation underlying Figure S3 are similar to those for S1 and S2 in our sample.

For the second and third phonon bands we find intersections $k_p = 2k_l$ at frequencies around 280GHz and 360GHz, that is, roughly 30-40GHz below and above the center of the second minigap. These are the two Brillouin backscattering peaks A and C reported in Fig. 2 of the main text. The first intersection $k_p = 2k_l$, which mainly reflects the bulk dispersion relation of GaAlAs, occurs around 30-40GHz. In our experimental configuration, its frequency is however too close to the laser line to be resolved.

References

- Lanzillotti-Kimura, N. D., Fainstein, A., Balseiro, C. A. & Jusserand, B. Phonon engineering with acoustic nanocavities: Theoretical considerations on phonon molecules, band structures, and acoustic Bloch oscillations. *Phys. Rev. B* **75**, 024301 (2007).
- Lamberti, F. R. *et al.* Nanomechanical resonators based on adiabatic periodicity-breaking in a superlattice. *Appl. Phys. Lett.* **111**, 173107 (2017).
- Esmann, M. *et al.* Topological nanophononic states by band inversion. *Phys. Rev. B* **97**, 155422 (2018).
- Rozas, G. *et al.* Lifetime of THz Acoustic Nanocavity Modes. *Phys. Rev. Lett.* **102**, 015502 (2009).
- Lacharmoise, P., Fainstein, A., Jusserand, B. & Thierry-Mieg, V. Optical cavity enhancement of light-sound interaction in acoustic phonon cavities. *Appl. Phys. Lett.* **84**, 3274–3276 (2004).
- Lanzillotti-Kimura, N. D., Fainstein, A., Jusserand, B. & Lemaître, A. Resonant Raman scattering of nanocavity-confined acoustic phonons. *Phys. Rev. B* **79**, 035404 (2009).
- Trigo, M., Bruchhausen, A., Fainstein, A., Jusserand, B. & Thierry-Mieg, V. Confinement of Acoustical Vibrations in a Semiconductor Planar Phonon Cavity. *Phys. Rev. Lett.* **89**, 227402 (2002).
- Lamberti, F. R. *et al.* Optomechanical properties of GaAs/AlAs micropillar resonators operating in the 18 GHz range. *Opt. Express* **25**, 24437–24447 (2017).
- Xiao, M. *et al.* Geometric phase and band inversion in periodic acoustic systems. *Nat. Phys.* **11**, 240–244 (2015).
- Bajoni, D. *et al.* Polariton parametric luminescence in a single micropillar. *Appl. Phys. Lett.* **90**, 051107 (2007).
- Michaelis de Vasconcellos, S. *et al.* Spatial, spectral, and polarization properties of coupled micropillar cavities. *Appl. Phys. Lett.* **99**, 101103 (2011).
- Bajoni, D. *et al.* Polariton Laser Using Single Micropillar GaAs-GaAlAs Semiconductor Cavities. *Phys. Rev. Lett.* **100**, 047401 (2008).
- Gerard, J.- & Gayral, B. Strong Purcell effect for InAs quantum boxes in three-dimensional solid-state microcavities. *J. Light. Technol.* **17**, 2089–2095 (1999).
- Gayral, B., Gérard, J. M., Legrand, B., Costard, E. & Thierry-Mieg, V. Optical study of GaAs/AlAs pillar microcavities with elliptical cross section. *Appl. Phys. Lett.* **72**, 1421–1423 (1998).
- Fainstein, A. & Jusserand, B. Raman Scattering in Resonant Cavities. in *Light Scattering in Solid IX* 17–110 (Springer, Berlin, Heidelberg, 2006). doi:10.1007/978-3-540-34436-0_2